

Numerical upscaling for wave equations with time-dependent multiscale coefficients*

Bernhard Maier[†] Barbara Verfürth[†]

Abstract. In this paper, we consider the classical wave equation with time-dependent, spatially multiscale coefficients. We propose a fully discrete computational multiscale method in the spirit of the localized orthogonal decomposition in space with a backward Euler scheme in time. We show optimal convergence rates in space and time beyond the assumptions of spatial periodicity or scale separation of the coefficients. Further, we propose an adaptive update strategy for the time-dependent multiscale basis. Numerical experiments illustrate the theoretical results and showcase the practicability of the adaptive update strategy.

Key words. wave equation, numerical homogenization, multiscale method, time-dependent multiscale coefficients, a priori estimates

AMS subject classifications. 35L05, 65M15, 65M60, 65N30

Time-modulated metamaterials [3, 4] have recently received growing interest because of their astonishing physical properties such as the ability to break time-reversal symmetry [14, 24]. These can be modeled by the classical wave equation with space- and time-dependent coefficients. Additionally, the metamaterials are characterized by fine spatial structures, such that these coefficients are in general rapidly varying on small spatial scales. Besides time-modulated metamaterials, multiscale problems with time-dependent coefficients also occur in multiphysics simulations and for problems posed on evolving domains. Furthermore, similar difficulties also arise for nonlinear wave-type problems, cf. [21, 29, 32].

Wave equations with time-dependent coefficients that are slowly varying in space were studied with finite element space discretizations and various time integration schemes in [5, 6]. However, in the metamaterial context with spatially multiscale coefficients, standard finite element methods need to resolve all scales leading to an enormous and often impractical computational effort. Therefore, computational multiscale methods are suggested such as heterogeneous multiscale methods [1, 9], multiscale finite element methods [22, 23], and rough polyharmonic splines [33], to name a few.

*This work is funded by the German Research Foundation (DFG) – Project-ID 258734477 – SFB 1173 as well as by the Federal Ministry of Education and Research (BMBF) and the Baden-Württemberg Ministry of Science as part of the Excellence Strategy of the German Federal and State Governments.

[†]Institut für Angewandte und Numerische Mathematik, Karlsruher Institut für Technologie, Englerstr. 2, D-76131 Karlsruhe, {bernhard.maier, barbara.verfuerth}@kit.edu

In the present paper, we study wave equations with time-dependent multiscale coefficients, i.e., coefficients with a continuum of spatial scales that are only slowly evolving in time. We propose a fully discrete computational multiscale method in the spirit of the Localized Orthogonal Decomposition (LOD) [20, 27, 28] with a backward Euler scheme for the time integration. The LOD was successfully applied to time-harmonic wave propagation problems such as the Helmholtz equation, e.g., in [11, 31, 34, 36], and Maxwell's equation [10, 19]. Wave equations with time-invariant multiscale coefficients were studied in [2], using the implicit Crank–Nicolson scheme for the integration in time. In [12, 30, 35] these results were extended to the explicit leapfrog scheme including mass lumping to further enhance the computational efficiency. The presence of strong damping is considered in [25].

Our main contribution is the first rigorous fully discrete a priori error analysis of the LOD for the wave equation with time-dependent coefficients. We combine techniques for time-invariant multiscale [2] and smooth time-dependent [5] coefficients in order to prove the expected order of convergence in space and time. We strongly emphasize that merging these frameworks requires additional sophisticated concepts. For instance, we prove exponential decay of time derivatives of the correction operators and rely on a special projection onto the multiscale space, which is not the usual Ritz projection. Moreover, to enhance the computational efficiency of our scheme, we further propose an adaptive update strategy for the time-dependent multiscale basis using error indicators in the spirit of [16, 17].

Our paper is organized as follows. In Section 1 we introduce the wave equation with time-dependent multiscale coefficients and our basic assumptions. Section 2 consists of two parts, where we first review the main concepts of the LOD and highlight the additional difficulties due to the time-dependent coefficients. Finally, we present the fully discrete numerical scheme and state our main error result. Subsequently, we provide a rigorous proof for this a priori error estimate in Section 3. In Section 4 we propose a Petrov–Galerkin variant of our scheme and introduce the adaptive update strategy. We conclude with numerical experiments that confirm our theoretical findings in Section 5.

1 Setting

For $T > 0$ and a bounded polyhedral Lipschitz domain $\Omega \subset \mathbb{R}^d$, $d \in \mathbb{N}$, we consider the wave equation with time-dependent multiscale coefficients

$$\begin{cases} \partial_{tt}u_\varepsilon(t, x) = \nabla \cdot (a_\varepsilon(t, x) \nabla u_\varepsilon(t, x)) + f(t, x), & t \in [0, T], x \in \Omega, \\ u_\varepsilon(t, x) = 0, & t \in [0, T], x \in \partial\Omega, \\ u_\varepsilon(0, x) = u^0, \quad \partial_t u_\varepsilon(0, x) = v^0, & x \in \Omega, \end{cases} \quad (1.1)$$

with given initial values $u^0, v^0 \in H_0^1(\Omega)$ and right-hand side $f \in C^1([0, T], L^2(\Omega))$. We assume that there are constants $c_a, C_a, C_a^{\partial_t} > 0$ which are in particular independent of $0 < \varepsilon \ll 1$ such that the time-dependent multiscale parameter $a_\varepsilon \in C^1([0, T], L^\infty(\Omega))$

satisfies

$$c_a \leq a_\varepsilon(t, x) \leq C_a, \quad |\partial_t a_\varepsilon(t, x)| \leq C_a^{\partial_t}, \quad (1.2)$$

for all $t \in [0, T]$ and almost every $x \in \Omega$. We emphasize that we do not assume a_ε to be regular in space, since this would contradict the multiscale structure of a_ε . We use the subscript ε to stress the multiscale nature of quantities, but assume neither periodicity nor scale separation.

Remark 1.1. *Note that for the sake of simplicity we only consider scalar-valued coefficients a_ε here, but all arguments also extend to a_ε being a symmetric matrix-valued coefficient. Further, we point out that wellposedness of (1.1) is shown in [13] under compatibility conditions on the initial data, i.e., on u^0, v^0 , and $f(0, \cdot)$. In particular, for vanishing initial data and $f \in W^{2,1}([0, T], L^2(\Omega))$, there exists a unique solution u_ε of (1.1) satisfying*

$$u_\varepsilon \in C^3([0, T], L^2(\Omega)) \cap C^2([0, T], H_0^1(\Omega)).$$

We introduce the Hilbert spaces

$$\begin{aligned} \mathcal{H} &= L^2(\Omega), & (\varphi | \psi)_{\mathcal{H}} &= (\varphi | \psi)_{L^2(\Omega)}, \\ \mathcal{V} &= H_0^1(\Omega), & (\varphi | \psi)_{\mathcal{V}} &= (\nabla \varphi | \nabla \psi)_{L^2(\Omega)}. \end{aligned}$$

Moreover, for $t \in [0, T]$ we use the time-dependent weighted inner product

$$(\varphi | \psi)_{\mathcal{V}(t), D} = (a_\varepsilon(t, \cdot) \nabla \varphi | \nabla \psi)_{L^2(D)}, \quad D \subset \Omega,$$

which is well defined due to (1.2). For $D = \Omega$ we omit the subscript and simply write $(\cdot | \cdot)_{\mathcal{V}(t)}$. Note that (1.2) implies the norm equivalence

$$c_a \|\varphi\|_{\mathcal{V}}^2 \leq \|\varphi\|_{\mathcal{V}(t)}^2 \leq C_a \|\varphi\|_{\mathcal{V}}^2. \quad (1.3)$$

We further define the product spaces $\mathcal{X} = \mathcal{V} \times \mathcal{H}$ and $\mathcal{X}(t) = \mathcal{V}(t) \times \mathcal{H}$.

Based on these spaces, we study (1.1) with $y_\varepsilon = (u_\varepsilon, \partial_t u_\varepsilon)$ as the first-order Cauchy problem

$$\begin{cases} \partial_t y_\varepsilon(t) = \mathcal{A}_\varepsilon(t) y_\varepsilon(t) + \mathcal{F}(t), & t \in [0, T], \\ y_\varepsilon(0) = y^0, \end{cases} \quad (1.4)$$

with the initial value $y^0 = (u^0, v^0)$, the right-hand side $\mathcal{F} = (0, f)$, and the time-dependent operator

$$\mathcal{A}_\varepsilon(t): D(\mathcal{A}_\varepsilon(t)) \rightarrow \mathcal{X}, \quad \mathcal{A}_\varepsilon(t) \begin{pmatrix} \varphi_1 \\ \varphi_2 \end{pmatrix} = \begin{pmatrix} \varphi_2 \\ \nabla \cdot (a_\varepsilon(t, \cdot) \nabla \varphi_1) \end{pmatrix},$$

for $t \in [0, T]$. In particular, this implies for $\varphi = (\varphi_1, \varphi_2), \psi = (\psi_1, \psi_2)$

$$(\mathcal{A}_\varepsilon(t) \varphi | \psi)_{\mathcal{X}(t)} = (\varphi_2 | \psi_1)_{\mathcal{V}(t)} - (\varphi_1 | \psi_2)_{\mathcal{V}(t)}.$$

2 Fully discrete localized orthogonal decomposition

At the end of this section, we propose a fully discrete numerical scheme for the wave equation with time-dependent multiscale coefficients (1.1). To this end, we first introduce the spatially discrete setting in the spirit of the LOD in the first subsection. We then state the fully discrete scheme and our main result, which yields wellposedness as well as a rigorous error estimate.

2.1 Localized orthogonal decomposition

For time-invariant multiscale coefficients, the LOD is a well-established approach to improve the computational efficiency of numerical schemes. In particular, we refer to [28] for a detailed introduction to the topic. However, in our setting additional difficulties arise due to the dependency of the multiscale coefficient on time. Thus, we review the main ideas of the LOD in the following and highlight the additional difficulties. Overall, we mostly stick to the notation of [26].

Let $\{\mathcal{T}_h\}_{h>0}$ and $\{\mathcal{T}_H\}_{H>h}$ be two families of shape-regular and quasi-uniform triangulations of Ω , with h and H denoting the respective mesh width. Moreover, let W_h and W_H be the corresponding finite element spaces consisting of Lagrange elements of lowest order. In the following, we always assume that \mathcal{T}_h is a refinement of \mathcal{T}_H such that $W_H \subset W_h$ is satisfied.

Further, since the construction of the scheme is built on quasi-local projections, we recursively define for $K \in \mathcal{T}_H$ the patch of size $k \in \mathbb{N}_0$ by

$$N_0(K) = K, \quad N_k(K) = \bigcup_{K \in \mathcal{T}_H} \left\{ \overline{K} \cap \overline{N_{k-1}(K)} \neq \emptyset \right\}. \quad (2.1)$$

Fine finite element space In the following, we assume that the fine mesh width h is chosen sufficiently small such that all oscillations of a_ε are resolved. Thus, based on W_h the standard finite element method is applicable. However, due to the smallness of ε and the associated high dimension of W_h , this is computationally at least very costly, if possible at all. Nevertheless, we introduce the scheme here, since this is used as the reference solution in the error estimates for our multiscale scheme. We emphasize that this reference solution is not needed for our scheme and is never computed in practice.

Based on the fine space W_h , we define the Hilbert spaces $\mathcal{H}_h = W_h$, $\mathcal{V}_h = W_h$, equipped with the inner product of \mathcal{H} and \mathcal{V} , respectively. Additionally, we introduce the product space $\mathcal{X}_h = \mathcal{V}_h \times \mathcal{H}_h$. We consider the discrete first-order Cauchy problem

$$\begin{cases} \partial_t y_h(t) = \mathcal{A}_h(t)y_h(t) + \mathcal{F}_h(t), & t \in [0, T], \\ y_h(0) = y_h^0. \end{cases} \quad (2.2)$$

For $t \in [0, T]$ the time-dependent operator $\mathcal{A}_h(t): \mathcal{X}_h \rightarrow \mathcal{X}_h$ is given by

$$\mathcal{A}_h(t) \begin{pmatrix} \varphi_1 \\ \varphi_2 \end{pmatrix} = \begin{pmatrix} \varphi_2 \\ -A_h(t)\varphi_1 \end{pmatrix},$$

where the operator $A_h(t): \mathcal{V}_h \rightarrow \mathcal{H}_h$ satisfies

$$(A_h(t)\varphi_1 | \psi_2)_{\mathcal{H}} = (\varphi_1 | \psi_2)_{\mathcal{V}(t)}, \quad \varphi_1, \psi_2 \in \mathcal{V}_h. \quad (2.3)$$

In general A_h is not uniformly bounded with respect to h . Nevertheless, this implies

$$(\mathcal{A}_h(t)\varphi | \psi)_{\mathcal{X}(t)} = (\varphi_2 | \psi_1)_{\mathcal{V}(t)} - (\varphi_1 | \psi_2)_{\mathcal{V}(t)}, \quad \varphi, \psi \in \mathcal{X}_h. \quad (2.4)$$

Moreover, the initial value $y_h^0 \in \mathcal{X}_h$ and the right-hand side $f_h: [0, T] \rightarrow \mathcal{H}_h$ approximate y^0 and f , respectively, and we set $\mathcal{F}_h = (0, f_h)$. Note that the wellposedness analysis in [13] also extends to the spatially discrete setting (2.2).

Coarse finite element space Correspondingly, for the coarse space W_H we introduce the Hilbert spaces $\mathcal{H}_H = W_H$, $\mathcal{V}_H = W_H$, $\mathcal{X}_H = \mathcal{V}_H \times \mathcal{H}_H$. Moreover, we introduce a projection $I_H \in \mathcal{L}(\mathcal{V}_h, \mathcal{V}_H)$, which satisfies for $K \in \mathcal{T}_H$ the bounds

$$\|\varphi - I_H\varphi\|_{\mathcal{H}, K} \leq C_I H \|\varphi\|_{\mathcal{V}, N_1(K)}, \quad \|\varphi - I_H\varphi\|_{\mathcal{V}, K} \leq C_I \|\varphi\|_{\mathcal{V}, N_1(K)}, \quad \varphi \in \mathcal{V}_h,$$

with a constant $C_I > 0$ depending on the regularity of the mesh, but independent of H . In particular, this implies the global bounds

$$\|\varphi - I_H\varphi\|_{\mathcal{H}} \lesssim CH \|\varphi\|_{\mathcal{V}}, \quad \|\varphi - I_H\varphi\|_{\mathcal{V}} \lesssim C \|\varphi\|_{\mathcal{V}}, \quad \varphi \in \mathcal{V}_h. \quad (2.5)$$

Moreover, we assume that I_H is not only stable in \mathcal{V} , but also in \mathcal{H} , i.e., we rely on

$$\|I_H\varphi\|_{\mathcal{H}} \lesssim C \|\varphi\|_{\mathcal{H}}, \quad \varphi \in \mathcal{H}_h. \quad (2.6)$$

Note that the quasi-interpolation operator introduced in [28, Chap. 3.3], which is also known as the Oswald operator, is a suitable choice for I_H satisfying our assumptions.

Based on I_H we decompose the fine space $\mathcal{V}_h = \mathcal{V}^f \oplus \mathcal{V}_H$, where $\mathcal{V}^f = \ker I_H$ and the dimension of \mathcal{V}_H is sufficiently small such that it allows for the construction of a computationally efficient scheme. However, we point out that this decomposition is not orthogonal with respect to the inner product of \mathcal{V}_h and thus \mathcal{V}_H is not an optimal approximation space.

Time-dependent multiscale space We now enhance the coarse space W_H to get an orthogonal decomposition of \mathcal{V}_h with respect to the time-dependent inner product of $\mathcal{V}(t)$. To this end, we introduce the time-dependent orthogonal projection $R_f(t) \in \mathcal{L}(\mathcal{V}_h, \mathcal{V}^f)$ given by

$$(R_f(t)\varphi | \psi)_{\mathcal{V}(t)} = (\varphi | \psi)_{\mathcal{V}(t)}, \quad t \in [0, T], \varphi \in \mathcal{V}_h, \psi \in \mathcal{V}^f. \quad (2.7)$$

Furthermore, we make use of the corresponding mapping for time-dependent functions $R_f: C^1([0, T], \mathcal{V}_h) \rightarrow C^1([0, T], \mathcal{V}^f)$, which is well defined due to the regularity (1.2) of a_ε in time. The time-dependent multiscale space is then defined by

$$\mathcal{V}_{\text{ms}}(t) = (\text{Id} - R_f(t))\mathcal{V}_H, \quad t \in [0, T]. \quad (2.8)$$

Note that for all $t \in [0, T]$ we have the orthogonal decomposition $\mathcal{V}_h = \mathcal{V}_{\text{ms}}(t) \oplus \mathcal{V}^f$ with respect to $(\cdot | \cdot)_{\mathcal{V}(t)}$.

We define for $t \in [0, T]$ the orthogonal projection $R_{\text{ms}}(t) \in \mathcal{L}(\mathcal{V}_h, \mathcal{V}_{\text{ms}}(t))$ by

$$(R_{\text{ms}}(t)\varphi | \psi)_{\mathcal{V}(t)} = (\varphi | \psi)_{\mathcal{V}(t)}, \quad t \in [0, T], \varphi \in \mathcal{V}_h, \psi \in \mathcal{V}_{\text{ms}}(t). \quad (2.9)$$

As before, we also introduce the corresponding mapping for time-dependent functions $R_{\text{ms}}: C^1([0, T], \mathcal{V}_h) \rightarrow C^1([0, T], \mathcal{V}_h)$. In particular, we have $R_{\text{ms}} = \text{Id} - R_f$.

Localized time-dependent multiscale space Since $R_f(t)$ is globally defined on Ω , the multiscale space $\mathcal{V}_{\text{ms}}(t)$ in general consists of functions with global support and thus is not suited for the construction of an efficient numerical scheme. To circumvent this issue, we consider the element-wise contributions $R_{f,K}(t): \mathcal{V}_h \rightarrow \mathcal{V}^f$ given by

$$(R_{f,K}(t)\varphi | \psi)_{\mathcal{V}(t)} = (\varphi | \psi)_{\mathcal{V}(t),K}, \quad K \in \mathcal{T}_H, t \in [0, T], \varphi \in \mathcal{V}_h, \psi \in \mathcal{V}^f. \quad (2.10)$$

In particular, (2.7) implies $R_f = \sum_{K \in \mathcal{T}_H} R_{f,K}$. As shown for instance in [28, Chap. 4.1], $R_{f,K}\varphi$ decays exponentially. Moreover, in Proposition 3.3 we show that this also holds for the time derivatives $\partial_t(R_{f,K}\varphi)$. This motivates the localization of R_f , R_{ms} , and $\mathcal{V}_{\text{ms}}(t)$.

Based on the notation introduced in (2.1), the localized element-wise contributions $R_{f,k,K}(t): \mathcal{V}_h \rightarrow \mathcal{V}^f(N_k(K))$ are given by

$$(R_{f,k,K}(t)\varphi | \psi)_{\mathcal{V}(t),N_k(K)} = (\varphi | \psi)_{\mathcal{V}(t),K}, \quad t \in [0, T], \varphi \in \mathcal{V}_h, \psi \in \mathcal{V}^f(N_k(K)), \quad (2.11)$$

using the localized fine space $\mathcal{V}^f(N_k(K)) = \{\varphi \in \mathcal{V}^f \mid \text{supp } \varphi \subset N_k(K)\}$.

Recombination yields the localized projection $R_{f,k} = \sum_{K \in \mathcal{T}_H} R_{f,k,K}$. Again, we also use the mapping for time-dependent functions $R_{f,k}: C^1([0, T], \mathcal{V}_h) \rightarrow C^1([0, T], \mathcal{V}^f)$. Moreover, similarly to (2.8) and (2.9) we define the localized time-dependent multiscale space

$$\mathcal{V}_{k,\text{ms}}(t) = (\text{Id} - R_{f,k}(t))\mathcal{V}_H, \quad t \in [0, T], \quad (2.12)$$

and $R_{k,\text{ms}}(t) \in \mathcal{L}(\mathcal{V}_h, \mathcal{V}_{k,\text{ms}}(t))$ as well as $R_{k,\text{ms}}: C^1([0, T], \mathcal{V}_h) \rightarrow C^1([0, T], \mathcal{V}_h)$ via

$$(R_{k,\text{ms}}(t)\varphi | \psi)_{\mathcal{V}(t)} = (\varphi | \psi)_{\mathcal{V}(t)}, \quad t \in [0, T], \varphi \in \mathcal{V}_h, \psi \in \mathcal{V}_{k,\text{ms}}(t).$$

Additionally, we introduce $\tilde{R}_{k,\text{ms}}(t) \in \mathcal{L}(\mathcal{V}_h, \mathcal{V}_{k,\text{ms}}(t))$ and correspondingly for time-dependent functions $\tilde{R}_{k,\text{ms}}: C^1([0, T], \mathcal{V}_h) \rightarrow C^1([0, T], \mathcal{V}_h)$ by

$$\tilde{R}_{k,\text{ms}} = (\text{Id} - R_{f,k})I_H. \quad (2.13)$$

In contrast to the (Ritz) projection $R_{k,\text{ms}}$, the projection $\tilde{R}_{k,\text{ms}}$ is not orthogonal to $\mathcal{V}_{k,\text{ms}}(t)$ with respect to the inner product of $\mathcal{V}(t)$. We emphasize that, nevertheless, the structure of $\tilde{R}_{k,\text{ms}}$ is very similar to the ideal multiscale projection $R_{\text{ms}} = \text{Id} - R_f$. This is a key aspect of our error analysis.

Finally, we introduce the space $\mathcal{H}_{k,\text{ms}}(t)$ consisting of the same functions as $\mathcal{V}_{k,\text{ms}}(t)$, but equipped with the inner product of \mathcal{H} , as well as $\mathcal{X}_{k,\text{ms}}(t) = \mathcal{V}_{k,\text{ms}}(t) \times \mathcal{H}_{k,\text{ms}}(t)$. The corresponding time-dependent multiscale projections $P_{k,\text{ms}}(t) \in \mathcal{L}(\mathcal{H}_h, \mathcal{H}_{k,\text{ms}}(t))$ and $P_{k,\text{ms}}: C^1([0, T], \mathcal{H}_h) \rightarrow C^1([0, T], \mathcal{H}_h)$ satisfy

$$(P_{k,\text{ms}}(t)\varphi \mid \psi)_{\mathcal{H}} = (\varphi \mid \psi)_{\mathcal{H}}, \quad t \in [0, T], \varphi \in \mathcal{H}_h, \psi \in \mathcal{H}_{k,\text{ms}}(t).$$

Remark 2.1. *The time-dependency of a_ε requires the multiscale spaces to be time-dependent as well, which largely influences the fully discrete scheme and its error analysis below. In the special case where $a_\varepsilon(t, x) = a_{1,\varepsilon}(x)a_2(t)$, the localized element projections $R_{\mathbb{f},k,K}(t)$ in (2.11) can be equivalently formulated with $a_{1,\varepsilon}$ only, so that they become time-independent. Hence, in this special case, we can work with time-independent multiscale spaces and the following error analysis can be simplified. We illustrate this fact also in the numerical experiments.*

2.2 Fully discrete scheme

Following the method-of-lines approach, we now present the fully discrete localized orthogonal decomposition method for the wave equation with time-dependent multiscale coefficients (1.4) based on the backward Euler scheme for the discretization in time. To this end, let $\tau > 0$ denote the fixed time step, $N \in \mathbb{N}$ with $N\tau \leq T$, and $t_m = m\tau$ for all $m \leq N$. We introduce for $m = 0, \dots, N$ the short notation $\mathcal{X}^m = \mathcal{X}(t_m)$, $\mathcal{X}_{k,\text{ms}}^m = \mathcal{X}_{k,\text{ms}}(t_m)$, and the projections $\mathcal{P}_{k,\text{ms}}^m, \tilde{\mathcal{R}}_{k,\text{ms}}^m \in \mathcal{L}(\mathcal{X}_h, \mathcal{X}_{k,\text{ms}}^m)$ given by

$$\mathcal{P}_{k,\text{ms}}^m = \begin{pmatrix} R_{k,\text{ms}}(t_m) \\ P_{k,\text{ms}}(t_m) \end{pmatrix}, \quad \tilde{\mathcal{R}}_{k,\text{ms}}^m = \begin{pmatrix} \tilde{R}_{k,\text{ms}}(t_m) \\ \tilde{R}_{k,\text{ms}}(t_m) \end{pmatrix}. \quad (2.14)$$

Moreover, we define

$$\mathcal{A}_{k,\text{ms}}^m = \mathcal{P}_{k,\text{ms}}^m \mathcal{A}_h(t_m), \quad \mathcal{F}_{k,\text{ms}}^m = \mathcal{P}_{k,\text{ms}}^m \mathcal{F}_h(t_m), \quad y_{k,\text{ms}}^0 = \mathcal{P}_{k,\text{ms}}^0 y_h^0. \quad (2.15)$$

The fully discrete scheme then reads

$$y_{k,\text{ms}}^{n+1} = \mathcal{P}_{k,\text{ms}}^{n+1} y_{k,\text{ms}}^n + \tau \mathcal{A}_{k,\text{ms}}^{n+1} y_{k,\text{ms}}^{n+1} + \tau \mathcal{F}_{k,\text{ms}}^{n+1}, \quad n = 0, \dots, N-1. \quad (2.16)$$

Note that we apply the projection $\mathcal{P}_{k,\text{ms}}^{n+1}$ to the previous approximation $y_{k,\text{ms}}^n$ in order to ensure $y_{k,\text{ms}}^{n+1} \in \mathcal{X}_{k,\text{ms}}^{n+1}$. Thus, the right-hand side of (2.16) is well defined.

We now state our main result, which yields wellposedness and a rigorous error estimate for the fully discrete scheme.

Theorem 2.2. *Let $y_h = (u_h, \partial_t u_h)$ be the solution of (2.2) with*

$$u_h \in C^3([0, T], \mathcal{H}_h) \cap C^2([0, T], \mathcal{V}_h) \quad (2.17)$$

bounded independent of ε . Moreover, let $k \geq (1 + \frac{d}{2})|\log H|/|\log \mu|$. Then, the approximations $y_{k,\text{ms}}^n = (u_{k,\text{ms}}^n, v_{k,\text{ms}}^n)$ obtained by the fully discrete localized orthogonal decomposition method (2.16) for the wave equation with time-dependent multiscale coefficients (1.4) satisfy for $n = 1, \dots, N$ the error estimate

$$\|u_{k,\text{ms}}^n - u_h(t_n)\|_{\mathcal{V}} + \|v_{k,\text{ms}}^n - \partial_t u_h(t_n)\|_{\mathcal{H}} \leq C_{u,f} e^{C_a t_n} (\tau + H),$$

where the constants $C_{u,f}, C_a > 0$ depend on $c_a, C_a, C_a^{\partial_t}$, and the mesh regularity, but not on the variations of a_ε . Further, $C_{u,f}$ depends on (2.17), but not on ε . The constant $0 < \mu < 1$ is given by Proposition 3.3.

The proof of the main result is given at the end of the next section. We conclude this section with the following remarks.

Remark 2.3. As stated in Remark 1.1, wellposedness of wave equations with time-dependent coefficients of the form (1.4) and (2.2) is studied in [13]. In particular, the author derives compatibility conditions on the initial data and the right-hand side such that the regularity assumption (2.17) on u_h holds. In order to have ε -independent a priori bounds on u_h in the associated norms, it is additionally required that the initial values and the right-hand side satisfy ε -independent bounds in appropriate norms, cf. [2] for a detailed discussion in the case of time-independent a_ε . For instance, it is shown in [13] that the assumption of well-prepared data is satisfied for vanishing initial data and $f_h \in W^{2,1}([0, T], \mathcal{H}_h)$.

Remark 2.4. Similar arguments as in the proof of Theorem 2.2 also yield an error estimate for the spatially discrete problem without the discretization in time. However, since wellposedness thereof is much more involved, we refrain from presenting the details here.

Remark 2.5. We emphasize that our analysis for the backward Euler scheme offers a good starting point for the derivation of higher-order schemes. For instance, correspondingly to (2.16) we propose the following fully discrete scheme for the wave equation with time-dependent multiscale coefficients (1.4) based on the implicit midpoint rule, which is given by

$$\begin{aligned} y_{k,\text{ms}}^{n+1/2} &= \mathcal{P}_{k,\text{ms}}^{n+1/2} y_{k,\text{ms}}^n + \frac{\tau}{2} \mathcal{A}_{k,\text{ms}}^{n+1/2} y_{k,\text{ms}}^{n+1/2} + \frac{\tau}{2} \mathcal{F}_{k,\text{ms}}^{n+1/2}, \\ y_{k,\text{ms}}^{n+1} &= 2y_{k,\text{ms}}^{n+1/2} - y_{k,\text{ms}}^n, \end{aligned} \quad n = 0, \dots, N-1. \quad (2.18)$$

The discrete operators are defined as in (2.14) and (2.15) with $t_{m+1/2} = t_m + \frac{\tau}{2}$. In particular, (2.18) implies $y_{k,\text{ms}}^{n+1/2} \in \mathcal{X}_{k,\text{ms}}^{n+1/2}$, which is crucial for the right-hand side to be well defined, but not $y_{k,\text{ms}}^{n+1} \in \mathcal{X}_{k,\text{ms}}^{n+1}$. We point out that in our numerical experiments in Section 5 this scheme is second-order convergent. However, since the corresponding analysis is much more involved, we focus in the present paper on the analysis of the backward Euler scheme.

3 Error analysis

The aim of this section is to provide a rigorous proof for our main result Theorem 2.2. To this end, in the first subsection we investigate the approximation properties of the projection operators. Based on these estimates, we finally conclude an error estimate for the fully discrete scheme in the second subsection.

3.1 Approximation properties of projections

In the following, we study the projections introduced in Section 2.1. In particular, this includes the derivation of estimates for the corresponding time derivatives.

To begin with, the definition (2.13) of $\tilde{R}_{k,\text{ms}}$ and the identity $R_{\text{ms}}(\text{Id} - I_H) = 0$ in \mathcal{V}_h imply

$$\tilde{R}_{k,\text{ms}} - \text{Id} = R_{\text{ms}} - \text{Id} + (R_f - R_{f,k})I_H. \quad (3.1)$$

Thus, in the following lemmas we study the ideal multiscale projection R_{ms} and the perturbation error due to the localization $R_{f,k}$ of the finescale projection R_f . Finally, we conclude bounds for the non-orthogonal multiscale projection $\tilde{R}_{k,\text{ms}}$.

We start with the ideal multiscale projection R_{ms} introduced in (2.9).

Lemma 3.1. *Let $t \in [0, T]$ and $\varphi \in C^1([0, T], \mathcal{V}_h)$ with $A_h(t)\varphi(t) \in \mathcal{H}_h$. Then, we have*

$$\|(\text{Id} - R_{\text{ms}}(t))\varphi(t)\|_{\mathcal{V}} \lesssim H \|A_h(t)\varphi(t)\|_{\mathcal{H}}, \quad (3.2)$$

$$\|\partial_t((\text{Id} - R_{\text{ms}})\varphi)(t)\|_{\mathcal{V}} \lesssim H \left(\|A_h(t)\varphi(t)\|_{\mathcal{H}} + \|\partial_t(A_h(t)\varphi(t))\|_{\mathcal{H}} \right), \quad (3.3)$$

where the hidden constant might depend on c_a , C_a , $C_a^{\partial_t}$, and the mesh regularity, but not on the spatial variations of a_ε .

Proof. The estimate (3.2) follows directly from $R_f = \text{Id} - R_{\text{ms}}$, the norm equivalence (1.3), and (2.5). To prove (3.3), we first obtain due to $\partial_t(R_f\varphi) \in C^1([0, T], \mathcal{V}^f)$

$$\|\partial_t((\text{Id} - R_{\text{ms}})\varphi)(t)\|_{\mathcal{V}(t)} = \sup_{\substack{\psi \in \mathcal{V}^f \\ \|\psi\|_{\mathcal{V}(t)}=1}} (a_\varepsilon(t) \nabla \partial_t(R_f\varphi)(t) \mid \nabla \psi)_{\mathcal{H}}.$$

The product rule together with (2.7) implies

$$\begin{aligned} & (a_\varepsilon(t) \nabla \partial_t(R_f\varphi)(t) \mid \nabla \psi)_{\mathcal{H}} \\ &= \partial_t(a_\varepsilon(t) \nabla \varphi(t) \mid \nabla \psi)_{\mathcal{H}} - (\partial_t a_\varepsilon(t) \nabla (R_f(t)\varphi(t)) \mid \nabla \psi)_{\mathcal{H}}. \end{aligned} \quad (3.4)$$

For the first term, we derive with the definition (2.3) of A_h , $\psi \in \ker I_H$, and (2.5) the bound

$$\begin{aligned} |\partial_t(a_\varepsilon(t) \nabla \varphi(t) \mid \nabla \psi)_{\mathcal{H}}| &\leq \|\partial_t(A_h(t)\varphi(t))\|_{\mathcal{H}} \|(\text{Id} - I_H)\psi\|_{\mathcal{H}} \\ &\lesssim H \|\partial_t(A_h(t)\varphi(t))\|_{\mathcal{H}} \|\psi\|_{\mathcal{V}}. \end{aligned}$$

For the second term, the Cauchy–Schwarz inequality yields

$$(\partial_t a_\varepsilon(t) \nabla (R_f(t)\varphi(t)) \mid \nabla \psi)_{\mathcal{H}} \leq \|\partial_t a_\varepsilon(t)\|_{L^\infty(\Omega)} \|(\text{Id} - R_{\text{ms}}(t))\varphi(t)\|_{\mathcal{V}} \|\psi\|_{\mathcal{V}}.$$

Finally, (3.2) and the norm equivalence (1.3) conclude the proof. \square

Although $\|A_h(t)\varphi\|_{\mathcal{H}}$ is in general not uniformly bounded in h , we point out that the finite element solution $y_h = (u_h, \partial_t u_h) \in C^1([0, T], \mathcal{X}_h)$ of (2.2) satisfies

$$\|A_h(t)u_h(t)\|_{\mathcal{H}} = \|\partial_{tt}u_h(t) - f_h(t)\|_{\mathcal{H}}. \quad (3.5)$$

Thus, for $\varphi = u_h$ and $\mathcal{F}_h \in C([0, T], \mathcal{X}_h)$ the right-hand side of (3.2) is uniformly bounded in h . Moreover, taking the derivative of (2.2) with respect to time, we obtain

$$\|\partial_t(A_h(t)u_h(t))\|_{\mathcal{H}} = \|\partial_{ttt}u_h(t) - \partial_t f_h(t)\|_{\mathcal{H}}. \quad (3.6)$$

Thus, for $\varphi = u_h$ the right-hand side of (3.3) is also uniformly bounded in h if we have $y_h \in C^2([0, T], \mathcal{X}_h)$ and $\mathcal{F}_h \in C^1([0, T], \mathcal{X}_h)$.

However, note that for time-dependent multiscale coefficients the same trick is not feasible for $\varphi = \partial_t u_h$, since the product rule yields

$$\|A_h(t)\partial_t u_h(t)\|_{\mathcal{H}} = \|\partial_{ttt}u_h(t) - \partial_t f_h(t) - \partial_t(A_h(t))u_h(t)\|_{\mathcal{H}},$$

but $\|\partial_t(A_h(t))u_h(t)\|_{\mathcal{H}}$ is in general not uniformly bounded in h . Thus, we provide alternative bounds in the following lemma using only the energy norm on the right-hand side.

Lemma 3.2. *Let $t \in [0, T]$ and $\varphi \in C^1([0, T], \mathcal{V}_h)$. Then, we have*

$$\|(\text{Id} - R_{\text{ms}}(t))\varphi(t)\|_{\mathcal{H}} \lesssim H\|\varphi(t)\|_{\mathcal{V}}, \quad (3.7)$$

$$\|\partial_t((\text{Id} - R_{\text{ms}})\varphi)(t)\|_{\mathcal{H}} \lesssim H(\|\varphi(t)\|_{\mathcal{V}} + \|\partial_t\varphi(t)\|_{\mathcal{V}}), \quad (3.8)$$

where the hidden constant might depend on c_a , C_a , $C_a^{\partial_t}$, and the mesh regularity, but not on the spatial variations of a_ε .

Proof. The bound (3.7) follows from $R_f = \text{Id} - R_{\text{ms}}$, (2.5), and (2.7). Furthermore, we obtain with $R_f: C^1([0, T], \mathcal{V}_h) \rightarrow C^1([0, T], \mathcal{V}^f)$ and (2.5)

$$\|\partial_t(R_f\varphi)(t)\|_{\mathcal{H}} \lesssim H\|\partial_t(R_f\varphi)(t)\|_{\mathcal{V}}.$$

Since (1.3), (2.7), and (3.4) imply

$$\|\partial_t(R_f\varphi)(t)\|_{\mathcal{V}} \lesssim (\|\varphi(t)\|_{\mathcal{V}} + \|\partial_t\varphi(t)\|_{\mathcal{V}}),$$

we also have (3.8). \square

So far we only studied the ideal multiscale projection R_{ms} . In order to obtain similar bounds for the localized projection $\tilde{R}_{k,\text{ms}}$, we first study the error introduced by the localization.

Proposition 3.3. *Let $t \in [0, T]$ and $\varphi \in C^1([0, T], \mathcal{V}_h)$. There is a constant $0 < \mu < 1$ depending on $\frac{c_a}{C_a}$ such that*

$$\|(R_f(t) - R_{f,k}(t))\varphi(t)\|_{\mathcal{V}} \lesssim k^{d/2} \mu^k \|\varphi(t)\|_{\mathcal{V}}, \quad (3.9)$$

$$\|\partial_t((R_f - R_{f,k})\varphi)(t)\|_{\mathcal{V}} \lesssim H^{-d/2} \mu^k (\|\varphi(t)\|_{\mathcal{V}} + \|\partial_t \varphi(t)\|_{\mathcal{V}}). \quad (3.10)$$

The hidden constant might depend on c_a , C_a , $C_a^{\partial_t}$, and the mesh regularity, but not on the variations of a_ε .

Proof. The estimate (3.9) was shown for instance in [18, Lem. 3.6]. Thus, we focus on the proof of (3.10) in the following, which consists of three parts. In the first two parts, we show the local estimates

$$\|\partial_t(R_{f,K}\varphi)(t)\|_{\mathcal{V}, \Omega \setminus N_k(K)} \lesssim \mu^k (\|\varphi(t)\|_{\mathcal{V}, K} + \|\partial_t \varphi(t)\|_{\mathcal{V}, K}), \quad (3.11)$$

$$\|\partial_t((R_{f,K} - R_{f,k,K})\varphi)(t)\|_{\mathcal{V}} \lesssim \mu^k (\|\varphi(t)\|_{\mathcal{V}, K} + \|\partial_t \varphi(t)\|_{\mathcal{V}, K}). \quad (3.12)$$

In the last part, we then conclude the global estimate (3.10). Note that in the remainder of the proof we omit the time-dependency of functions for the sake of readability. Moreover, we refrain from specifying the element $K \in \mathcal{T}_H$ for each patch $N_k(K)$ whenever this is clear from the context.

Step 1: Proof of (3.11): A corresponding estimate for constant-in-time coefficients is shown in [28, Thm. 4.1]. In the following, we extend this result to time-dependent multiscale coefficients.

For $k \geq 4$ and $K \in \mathcal{T}_H$ fixed we introduce the cut-off function $\eta_1 \in \mathcal{V}_H$ with

$$\eta_1 = 0 \quad \text{in } N_{k-3}(K), \quad \eta_1 = 1 \quad \text{in } \Omega \setminus N_{k-2}(K).$$

Thus, we obtain for $\tilde{\varphi} = R_{f,K}\varphi$ the estimate

$$\begin{aligned} \|\partial_t \tilde{\varphi}\|_{\mathcal{V}(t), \Omega \setminus N_k}^2 &\leq (\partial_t \tilde{\varphi} \mid (\text{Id} - I_H)(\eta_1 \partial_t \tilde{\varphi}))_{\mathcal{V}(t)} + (\partial_t \tilde{\varphi} \mid I_H(\eta_1 \partial_t \tilde{\varphi}))_{\mathcal{V}(t)} \\ &\quad - (a_\varepsilon \nabla \partial_t \tilde{\varphi} \mid (\nabla \eta_1) \partial_t \tilde{\varphi})_{\mathcal{H}}. \end{aligned}$$

For the first term, we derive from (2.10) for $\psi \in \mathcal{V}^f$

$$\begin{aligned} (\partial_t(R_{f,K}\varphi) \mid \psi)_{\mathcal{V}(t)} &= (\partial_t \varphi \mid \psi)_{\mathcal{V}(t), K} + (\partial_t a_\varepsilon \nabla \varphi \mid \nabla \psi)_{\mathcal{H}, K} \\ &\quad - (\partial_t a_\varepsilon \nabla(R_{f,K}\varphi) \mid \nabla \psi)_{\mathcal{H}}. \end{aligned} \quad (3.13)$$

In particular, this yields for $\psi = (\text{Id} - I_H)(\eta_1 \partial_t \tilde{\varphi}) \in \mathcal{V}^f(\Omega \setminus N_{k-4}(K))$

$$\begin{aligned} (\partial_t \tilde{\varphi} \mid (\text{Id} - I_H)(\eta_1 \partial_t \tilde{\varphi}))_{\mathcal{V}(t)} &= -(\partial_t a_\varepsilon \nabla \tilde{\varphi} \mid \nabla \psi)_{\mathcal{H}} \\ &\lesssim \|\tilde{\varphi}\|_{\mathcal{V}, \Omega \setminus N_{k-4}} \|\partial_t \tilde{\varphi}\|_{\mathcal{V}, \Omega \setminus N_{k-4}}, \end{aligned}$$

where we used (2.5) in the last step. Since the other two terms can be bounded as in [28, Thm. 4.1], we obtain with constants $C_1, C_2 > 0$

$$\|\partial_t \tilde{\varphi}\|_{\mathcal{V}(t), \Omega \setminus N_k}^2 \leq C_1 \|\partial_t \tilde{\varphi}\|_{\mathcal{V}(t), N_k \setminus N_{k-4}}^2 + C_2 \|\tilde{\varphi}\|_{\mathcal{V}, \Omega \setminus N_{k-4}} \|\partial_t \tilde{\varphi}\|_{\mathcal{V}, \Omega \setminus N_{k-4}}.$$

The identity $N_k \setminus N_{k-4} = (\Omega \setminus N_{k-4}) \setminus (\Omega \setminus N_k)$ and Young's inequality for $\varepsilon > 0$ yield

$$\|\partial_t \tilde{\varphi}\|_{\mathcal{V}(t), \Omega \setminus N_k}^2 \leq \left(\frac{C_1}{1+C_1} + \frac{\varepsilon}{2}\right) \|\partial_t \tilde{\varphi}\|_{\mathcal{V}(t), \Omega \setminus N_{k-4}}^2 + \frac{1}{2\varepsilon} \left(\frac{C_2}{1+C_1}\right)^2 \|\tilde{\varphi}\|_{\mathcal{V}, \Omega \setminus N_{k-4}}^2.$$

Due to $\frac{C_1}{1+C_1} < 1$ there is ε sufficiently small such that using the previous argument repeatedly yields

$$\|\partial_t \tilde{\varphi}\|_{\mathcal{V}(t), \Omega \setminus N_k}^2 \leq \mu^{\lfloor k/4 \rfloor} \|\partial_t \tilde{\varphi}\|_{\mathcal{V}(t), \Omega}^2 + C_3 \sum_{i=1}^{\lfloor k/4 \rfloor} \mu^{i-1} \|\tilde{\varphi}\|_{\mathcal{V}, \Omega \setminus N_{k-4i}}^2,$$

for some $0 < \mu < 1$ and $C_3 > 0$. Thus, we finally obtain with

$$\|\partial_t \tilde{\varphi}\|_{\mathcal{V}} \lesssim \|\varphi\|_{\mathcal{V}, K} + \|\partial_t \varphi\|_{\mathcal{V}, K}$$

and the exponential decay of $\tilde{\varphi} = R_{t,K} \varphi$ from [28, Thm. 4.1] the estimate (3.11), which remains valid for $k < 4$.

Step 2: Proof of (3.12): For the second part, (2.11) implies for $\psi_k \in \mathcal{V}^f(N_k(K))$

$$\begin{aligned} (\partial_t(R_{f,k,K}\varphi) \mid \psi_k)_{\mathcal{V}(t)} &= (\partial_t \varphi \mid \psi_k)_{\mathcal{V}(t), K} + (\partial_t a_\varepsilon \nabla \varphi \mid \nabla \psi_k)_{\mathcal{H}, K} \\ &\quad - (\partial_t a_\varepsilon \nabla(R_{f,k,K}\varphi) \mid \nabla \psi_k)_{\mathcal{H}}. \end{aligned}$$

Together with (3.13), this yields for $w = (R_{f,K} - R_{f,k,K})\varphi$ and $\psi_k \in \mathcal{V}^f(N_k(K))$ due to $\tilde{\psi}_k = \partial_t(R_{f,k,K}\varphi) - \psi_k \in \mathcal{V}^f(N_k(K))$ the estimate

$$\begin{aligned} \|\partial_t w\|_{\mathcal{V}(t)}^2 &= \left(\partial_t w \mid \partial_t w + \tilde{\psi}_k\right)_{\mathcal{V}(t)} + \left(\partial_t a_\varepsilon \nabla w \mid \nabla \tilde{\psi}_k\right)_{\mathcal{H}} \\ &= (\partial_t w \mid \partial_t \tilde{\varphi} - \psi_k)_{\mathcal{V}(t)} + (\partial_t a_\varepsilon \nabla w \mid \nabla(\partial_t \tilde{\varphi} - \psi_k))_{\mathcal{H}} \\ &\quad - (\partial_t a_\varepsilon \nabla w \mid \nabla(\partial_t w))_{\mathcal{H}} \\ &\lesssim (\|\partial_t w\|_{\mathcal{V}} + \|w\|_{\mathcal{V}}) \|\partial_t \tilde{\varphi} - \psi_k\|_{\mathcal{V}} + \|w\|_{\mathcal{V}} \|\partial_t w\|_{\mathcal{V}}, \end{aligned}$$

where we used the Cauchy–Schwarz inequality together with the norm equivalence (1.3) and the regularity (1.2) of a_ε in the last step. Since ψ_k is arbitrary, we have shown

$$\|\partial_t w\|_{\mathcal{V}} \lesssim \|w\|_{\mathcal{V}} + \inf_{\psi_k \in \mathcal{V}^f(N_k)} \|\partial_t \tilde{\varphi} - \psi_k\|_{\mathcal{V}}.$$

Using the estimate for $w = (R_{f,K} - R_{f,k,K})\varphi$ from [28, Cor. 4.2], the first term is bounded by the right-hand side of (3.12). For the second term, without loss of generality let $k \geq 3$. We choose $\psi_k = (\text{Id} - I_H)(\eta_2 \partial_t \tilde{\varphi})$ with the cut-off function $\eta_2 \in \mathcal{V}_H$ with

$$\eta_2 = 1 \quad \text{in } N_{k-2}(K), \quad \eta_2 = 0 \quad \text{in } \Omega \setminus N_{k-1}(K).$$

The estimate (3.12) then follows with the same arguments as in the proof of [28, Cor. 4.2].

Step 3: Proof of (3.10): To obtain the global bound (3.10), we use (3.12) and the triangle inequality to get

$$\begin{aligned} \|\partial_t((R_f - R_{f,k})\varphi)\|_{\mathcal{V}} &\leq \sum_{K \in \mathcal{T}_H} \|\partial_t((R_{f,K} - R_{f,k,K})\varphi)\|_{\mathcal{V}} \\ &\lesssim \mu^k \sum_{K \in \mathcal{T}_H} (\|\varphi\|_{\mathcal{V},K} + \|\partial_t\varphi\|_{\mathcal{V},K}). \end{aligned}$$

Due to the mesh regularity, this yields (3.12). \square

Remark 3.4. *Compared to (3.9) the estimate (3.10) for the time derivative seems to be sub-optimal. However, we point out that due to the dominant exponential decay, this only mildly affects the patch size k ; e.g., the choice $k \geq (1 + \frac{d}{2})|\log H|/|\log \mu|$ in Theorem 2.2 is sufficient to ensure the optimal convergence rates of the fully discrete scheme. Nevertheless, in future research it might be possible to improve the estimate (3.10).*

Due to (3.1), we directly conclude approximation properties of the localized projection $\tilde{R}_{k,\text{ms}}$ based on the previous lemmas.

Corollary 3.5. *Let $t \in [0, T]$ and $\varphi \in C^1([0, T], \mathcal{V}_h)$. There is a constant $0 < \mu < 1$ depending on $\frac{c_a}{C_a}$ such that*

$$\|(\text{Id} - \tilde{R}_{k,\text{ms}}(t))\varphi(t)\|_{\mathcal{V}} \lesssim H\|A_h(t)\varphi\|_{\mathcal{H}} + k^{d/2}\mu^k\|\varphi(t)\|_{\mathcal{V}}, \quad (3.14)$$

$$\|(\text{Id} - \tilde{R}_{k,\text{ms}}(t))\varphi(t)\|_{\mathcal{H}} \lesssim (H + k^{d/2}\mu^k)\|\varphi(t)\|_{\mathcal{V}}, \quad (3.15)$$

$$\begin{aligned} \|\partial_t((\text{Id} - \tilde{R}_{k,\text{ms}})\varphi)(t)\|_{\mathcal{V}} &\lesssim H\left(\|A_h(t)\varphi(t)\|_{\mathcal{H}} + \|\partial_t(A_h(t)\varphi(t))\|_{\mathcal{H}}\right) \\ &\quad + H^{-d/2}\mu^k(\|\varphi(t)\|_{\mathcal{V}} + \|\partial_t\varphi(t)\|_{\mathcal{V}}), \end{aligned} \quad (3.16)$$

$$\|\partial_t((\text{Id} - \tilde{R}_{k,\text{ms}})\varphi)(t)\|_{\mathcal{H}} \lesssim (H + H^{-d/2}\mu^k)\left(\|\varphi(t)\|_{\mathcal{V}} + \|\partial_t\varphi(t)\|_{\mathcal{V}}\right). \quad (3.17)$$

The hidden constant might depend on c_a , C_a , $C_a^{\partial_t}$, and the mesh regularity, but not on the variations of a_ε .

We emphasize that (3.14) and (3.15) are also valid for the standard localized multiscale projection $R_{k,\text{ms}}$, cf. [26, Lem. 3.5]. However, up to our knowledge it is unclear whether this also extends to the estimates (3.16) and (3.17) for the time derivatives, even with Proposition 3.3 at hand. To circumvent this, in our analysis we rely on the non-orthogonal localized multiscale projection $\tilde{R}_{k,\text{ms}}$ instead.

3.2 Analysis of fully discrete localized orthogonal decomposition

Finally, we present the proof of our main result.

Proof of Theorem 2.2. Using a similar notation as in (2.15), i.e.,

$$y_h^m = y_h(t_m), \quad \mathcal{A}_h^m = \mathcal{A}_h(t_m), \quad \mathcal{F}_h^m = \mathcal{F}_h(t_m), \quad m = 0, \dots, N,$$

the solution $y_h = (u_h, \partial_t u_h)$ of (2.2) satisfies the perturbed scheme

$$y_h^{n+1} = y_h^n + \tau \mathcal{A}_h^{n+1} y_h^{n+1} + \tau \mathcal{F}_h^{n+1} + \tau \delta_{\text{BE}}^{n+1}, \quad n = 0, \dots, N-1,$$

with a defect given by

$$\delta_{\text{BE}}^{n+1} = \frac{1}{\tau} (y_h^{n+1} - \tilde{y}_h^n) + \partial_t y_h(t_{n+1}).$$

Thus, the multiscale error $e_{k,\text{ms}}^n = y_{k,\text{ms}}^n - \tilde{\mathcal{R}}_{k,\text{ms}}^n y_h^n$ satisfies the error recursion

$$e_{k,\text{ms}}^{n+1} - \mathcal{P}_{k,\text{ms}}^{n+1} e_{k,\text{ms}}^n = (\mathcal{P}_{k,\text{ms}}^{n+1} - \text{Id}) \tilde{\mathcal{R}}_{k,\text{ms}}^n y_h^n + \tau \mathcal{A}_{k,\text{ms}}^{n+1} e_{k,\text{ms}}^{n+1} + \tau G_{k,\text{ms}}^{n+1},$$

with the right-hand side

$$\begin{aligned} G_{k,\text{ms}}^{n+1} &= (\mathcal{A}_{k,\text{ms}}^{n+1} \tilde{\mathcal{R}}_{k,\text{ms}}^{n+1} - \mathcal{A}_h^{n+1}) y_h^{n+1} + \mathcal{F}_{k,\text{ms}}^{n+1} - \mathcal{F}_h^{n+1} - \delta_{\text{BE}}^{n+1} \\ &\quad + \frac{1}{\tau} \int_{t_n}^{t_{n+1}} \partial_t \left((\text{Id} - \tilde{\mathcal{R}}_{k,\text{ms}}(t)) y_h(t) \right) dt. \end{aligned} \quad (3.18)$$

Taking the inner product in $\mathcal{X}_{k,\text{ms}}^{n+1}$ with $e_{k,\text{ms}}^{n+1}$, we obtain with (2.4), (2.15), and Young's inequality

$$\|e_{k,\text{ms}}^{n+1}\|_{\mathcal{X}^{n+1}}^2 - \|e_{k,\text{ms}}^n\|_{\mathcal{X}^{n+1}}^2 \leq 2\tau \left(G_{k,\text{ms}}^{n+1} \mid e_{k,\text{ms}}^{n+1} \right)_{\mathcal{X}^{n+1}}.$$

To further bound the right-hand side, we first obtain due to the stability of $\tilde{\mathcal{R}}_{k,\text{ms}}$, (3.9), and (3.14) for $\varphi_h \in \mathcal{V}_h$ and $\psi_H \in \mathcal{V}_H$ the estimate

$$\begin{aligned} &\left((\tilde{\mathcal{R}}_{k,\text{ms}}^{n+1} - \text{Id}) \varphi_h \mid (R_f^{n+1} - R_{f,k}^{n+1}) \psi_H \right)_{\mathcal{V}^{n+1}} \\ &\lesssim k^{d/2} \mu^k \min \left\{ \|\varphi_h\|_{\mathcal{V}}, \left(H \|A_h(t_{n+1}) \varphi_h\|_{\mathcal{H}} + k^{d/2} \mu^k \|\varphi_h\|_{\mathcal{V}} \right) \right\} \|\psi_H\|_{\mathcal{V}}. \end{aligned} \quad (3.19)$$

We denote the finite element parts of the multiscale error $e_{k,\text{ms}}^{n+1} = (e_{k,\text{ms},u}^{n+1}, e_{k,\text{ms},v}^{n+1})$ by $e_{H,u}^{n+1}, e_{H,v}^{n+1} \in \mathcal{V}_H$, i.e., we have

$$e_{k,\text{ms},u}^{n+1} = (1 - R_{f,k}^{n+1}) e_{H,u}^{n+1}, \quad e_{k,\text{ms},v}^{n+1} = (1 - R_{f,k}^{n+1}) e_{H,v}^{n+1}.$$

Based on an inverse estimate, cf. [7, Thm. 4.5.11], and the stability (2.5) and (2.6) of I_H in \mathcal{V} and \mathcal{H} , respectively, we further have

$$\|e_{H,u}^{n+1}\|_{\mathcal{V}} \lesssim \|e_{k,\text{ms},u}^{n+1}\|_{\mathcal{V}}, \quad \|e_{H,v}^{n+1}\|_{\mathcal{V}} \lesssim H^{-1} \|e_{k,\text{ms},v}^{n+1}\|_{\mathcal{H}}.$$

Thus, for the choice $k \geq (1 + \frac{d}{2}) |\log H| / |\log \mu|$ we conclude with the Cauchy-Schwarz inequality, (3.1), and (3.19) for the first term of (3.18)

$$\begin{aligned} &\left((\mathcal{A}_{k,\text{ms}}^{n+1} \tilde{\mathcal{R}}_{k,\text{ms}}^{n+1} - \mathcal{A}_h^{n+1}) y_h^{n+1} \mid e_{k,\text{ms}}^{n+1} \right)_{\mathcal{X}^{n+1}} \\ &= \left((\tilde{\mathcal{R}}_{k,\text{ms}}^{n+1} - \text{Id}) v_h^{n+1} \mid (R_f^{n+1} - R_{f,k}^{n+1}) e_{H,u}^{n+1} \right)_{\mathcal{V}^{n+1}} \\ &\quad - \left((\tilde{\mathcal{R}}_{k,\text{ms}}^{n+1} - \text{Id}) u_h^{n+1} \mid (R_f^{n+1} - R_{f,k}^{n+1}) e_{H,v}^{n+1} \right)_{\mathcal{V}^{n+1}} \\ &\lesssim H \left(\|u_h^{n+1}\|_{\mathcal{V}} + \|\partial_t u_h^{n+1}\|_{\mathcal{V}} + \|A_h(t_{n+1}) u_h^{n+1}\|_{\mathcal{H}} \right) \|e_{k,\text{ms}}^{n+1}\|_{\mathcal{X}^{n+1}}. \end{aligned}$$

Moreover, (2.15) implies

$$\left(\mathcal{F}_{k,\text{ms}}^{n+1} - \mathcal{F}_h^{n+1} \mid e_{k,\text{ms}}^{n+1} \right)_{\mathcal{X}^{n+1}} = 0.$$

For the defect, we deduce with Taylor's theorem

$$\|\delta_{\text{BE}}^{n+1}\|_{\mathcal{X}^{n+1}} \lesssim \tau (\|\partial_{tt} u_h\|_{L^\infty([0,T],\mathcal{V})} + \|\partial_{ttt} u_h\|_{L^\infty([0,T],\mathcal{H})}).$$

Finally, we apply (3.16) and (3.17) together with the norm equivalence (1.3) to show

$$\begin{aligned} \|\partial_t \left((\text{Id} - \tilde{\mathcal{R}}_{k,\text{ms}}(t)) y_h(t) \right)\|_{\mathcal{X}(t)} &\lesssim H \left(\|A_h(t) u_h(t)\|_{\mathcal{H}} + \|\partial_t (A_h(t) u_h(t))\|_{\mathcal{H}} \right. \\ &\quad \left. + \|u_h(t)\|_{\mathcal{V}} + \|\partial_t u_h(t)\|_{\mathcal{V}} + \|\partial_{tt} u_h(t)\|_{\mathcal{V}} \right). \end{aligned}$$

Collecting all results in (3.18), we obtain with (3.5), (3.6), and Young's inequality

$$\|e_{k,\text{ms}}^{n+1}\|_{\mathcal{X}^{n+1}}^2 - \|e_{k,\text{ms}}^n\|_{\mathcal{X}^{n+1}}^2 \leq \tau \|e_{k,\text{ms}}^{n+1}\|_{\mathcal{X}^{n+1}}^2 + \tau \widehat{\mathcal{C}}_{u,f}^2 (\tau + H)^2,$$

for some ε -independent constant $\widehat{\mathcal{C}}_{u,f} > 0$ depending on the regularity assumptions (2.17). Further, since (1.2) implies

$$\|e_{k,\text{ms}}^n\|_{\mathcal{X}^{n+1}}^2 = \|e_{k,\text{ms}}^n\|_{\mathcal{X}^n}^2 + \int_{t_n}^{t_{n+1}} (\partial_t a_\varepsilon(t) \nabla e_{k,\text{ms},u}^n \mid \nabla e_{k,\text{ms},u}^n)_{\mathcal{H}} dt \leq e^{C_a^{\partial_t} \tau} \|e_{k,\text{ms}}^n\|_{\mathcal{X}^n}^2,$$

we have

$$\|e_{k,\text{ms}}^{n+1}\|_{\mathcal{X}_{k,\text{ms}}^{n+1}}^2 - e^{C_a^{\partial_t} \tau} \|e_{k,\text{ms}}^n\|_{\mathcal{X}_{k,\text{ms}}^n}^2 \leq \tau \|e_{k,\text{ms}}^{n+1}\|_{\mathcal{X}_{k,\text{ms}}^{n+1}}^2 + \tau \widehat{\mathcal{C}}_{u,f}^2 (\tau + H)^2.$$

Multiplying with $e^{-C_a^{\partial_t} t_{n+1}}$ and using this identity recursively for $n, \dots, 0$, we get

$$e^{-C_a^{\partial_t} t_{n+1}} \|e_{k,\text{ms}}^{n+1}\|_{\mathcal{X}^{n+1}}^2 \leq \|e_{k,\text{ms}}^0\|_{\mathcal{X}^0}^2 + \tau \sum_{r=0}^n e^{-C_a^{\partial_t} t_{r+1}} \|e_{k,\text{ms}}^{r+1}\|_{\mathcal{X}^{r+1}}^2 + t_{n+1} \widehat{\mathcal{C}}_{u,f}^2 (\tau + H)^2.$$

Finally, a discrete version of Gronwall's inequality shows

$$\|e_{k,\text{ms}}^{n+1}\|_{\mathcal{X}^{n+1}}^2 \leq e^{C_a t_{n+1}} \left(\|e_{k,\text{ms}}^0\|_{\mathcal{X}^0}^2 + t_{n+1} \widehat{\mathcal{C}}_{u,f}^2 (\tau + H)^2 \right).$$

This concludes the proof, since with the notation $y_h^0 = (u_h^0, v_h^0)$ the initial error satisfies due to (2.15) and (3.15) the estimate

$$\begin{aligned} \|e_{k,\text{ms}}^0\|_{\mathcal{X}^0}^2 &= \|(P_{k,\text{ms}}(0) - \tilde{R}_{k,\text{ms}}(0)) v_h^0\|_{\mathcal{H}}^2 \\ &\leq \left((\text{Id} - \tilde{R}_{k,\text{ms}}(0)) v_h^0 \mid (P_{k,\text{ms}}(0) - \tilde{R}_{k,\text{ms}}(0)) v_h^0 \right)_{\mathcal{H}} \\ &\lesssim H \|v_h^0\|_{\mathcal{V}} \|e_{k,\text{ms}}^0\|_{\mathcal{X}^0}. \end{aligned} \quad \square$$

4 Practical aspects

In the previous sections, we proved that our fully discrete scheme (2.16) for the wave equation with time-dependent multiscale coefficients is wellposed and first-order convergent. However, since the multiscale coefficient a_ε is time-dependent, we have to recompute all correctors (2.10) in each time step, which might become rather time-consuming in practice. To circumvent this, we modify (2.16) in the following two subsections. First, we propose a Petrov–Galerkin variant in the spirit of [8] to avoid products of multiscale functions thereby reducing the communication in the assembly of the mass and stiffness matrices of the discrete system. Furthermore, this allows for an adaptive update strategy, which significantly improves the computational efficiency, cf. [16, 17]. We work with the backward Euler time stepping scheme as before, but emphasize that the following derivations can be easily transferred to the implicit midpoint rule mentioned in Remark 2.5.

4.1 Petrov–Galerkin formulation

We introduce the Petrov–Galerkin formulation in the matrix-vector-notation. To do so, we denote the nodal basis of the coarse finite element space W_H by $\{\lambda_j\}_{j=1}^J$, i.e., there are grid points $\{x_j\}_{j=1}^J \subset \Omega$ such that $\lambda_i(x_j) = \delta_{ij}$, $i, j = 1, \dots, J$, where δ_{ij} denotes the Kronecker delta. Due to the structure of the localized multiscale space $\mathcal{V}_{k,\text{ms}}(t)$ (2.12), we identify any time-dependent function $\zeta: [0, T] \rightarrow \mathcal{V}_{k,\text{ms}}(t)$ with its time-dependent vector-valued representation $\underline{\zeta} = (\underline{\zeta}_1, \dots, \underline{\zeta}_J): [0, T] \rightarrow \mathbb{R}^J$, which is uniquely characterized by

$$\zeta(t) = \sum_{j=1}^J (\text{Id} - R_{f,k}(t)) \lambda_j \underline{\zeta}_j(t), \quad t \in [0, T].$$

For the Petrov–Galerkin variant of (2.16) we directly use the coarse finite element space \mathcal{V}_H instead of the time-dependent localized multiscale space $\mathcal{V}_{k,\text{ms}}(t)$ as the test space. To this end, we introduce for $m = 1, \dots, N$ the mass and stiffness matrices

$$\begin{aligned} \underline{M}_{ij}^m &= \sum_{K \in \mathcal{T}_H} (\underline{M}_K^m)_{ij} = \sum_{K \in \mathcal{T}_H} (\lambda_i | (\text{Id} - R_{f,k,K}^m) \lambda_j)_{L^2(N_k(K))}, \\ \underline{A}_{ij}^m &= \sum_{K \in \mathcal{T}_H} (\underline{A}_K^m)_{ij} = \sum_{K \in \mathcal{T}_H} (a_\varepsilon^m \nabla \lambda_i | \nabla ((\text{Id} - R_{f,k,K}^m) \lambda_j))_{L^2(N_k(K))}, \end{aligned} \quad i, j = 1, \dots, J,$$

based on the short notation $a_\varepsilon^m = a_\varepsilon(t_m, \cdot)$ and $R_{f,k,K}^m = R_{f,k,K}(t_m)$ for the multiscale coefficient and the localized correctors (2.11), respectively. For the first-order system, we further define

$$\underline{\mathcal{A}}^m = \begin{pmatrix} 0 & \underline{M}^m \\ -\underline{A}^m & 0 \end{pmatrix}, \quad \underline{\mathcal{M}}^m = \begin{pmatrix} \underline{M}^m & 0 \\ 0 & \underline{M}^m \end{pmatrix}.$$

Then, the solution of the Petrov–Galerkin variant of (2.16) is given by

$$z^m = \sum_{j=1}^J (\text{Id} - R_{f,k}^m) \lambda_j z_j^m, \quad m = 0, \dots, N,$$

where the vector-valued representations satisfy the recursion

$$\underline{\mathcal{M}}^{n+1} \underline{z}_i^{n+1} = \underline{\mathcal{M}}^{n+1} \underline{z}_i^n + \tau \underline{\mathcal{A}}_{ij}^{n+1} \underline{z}_j^{n+1} + \tau \underline{\mathcal{F}}_i^{n+1}, \quad n = 0, \dots, N-1. \quad (4.1)$$

For the initial value, we set $\underline{z}^0 = I_{Hyh}^0$. Further, we set $\underline{\mathcal{F}}_i^{n+1} = (f_h(t_{n+1}, \cdot) | \lambda_i)_{L^2(\Omega)}$.

Remark 4.1. Note that in (4.1), we slightly modified the projection of \underline{z}_i^n in comparison to (2.16). Namely, we use the finescale projection $R_{f,k,K}^{n+1}$ instead of projecting $(\text{Id} - R_{f,k,K}^n) \lambda_i \underline{z}_i^n$ onto $\mathcal{V}_{k,\text{ms}}^{n+1}$. This, however, is justified by the error estimates obtained through (3.9). In fact, one can even use the standard finite element mass matrix on the coarse mesh, see [30], and mass lumping is possible as well, see [12].

4.2 Adaptive update strategy

As a remedy for the recomputation of all correctors in each time step, we propose an adaptive update strategy for the correctors and LOD matrices that will be investigated in detail in the numerical experiments. The strategy is based on the following local error indicators. Let $a_\varepsilon^i = a_\varepsilon(t_i, \cdot)$ and $a_\varepsilon^n = a_\varepsilon(t_n, \cdot)$ be the coefficients at two different time instances with associated correctors $R_{f,k}^i$ and $R_{f,k}^n$. For any element K , we denote by

$$\bar{a}_{N_k(K)}(t) = |N_k(K)|^{-1} \int_{N_k(K)} a_\varepsilon(t, x) \, dx$$

the local average of a_ε and by

$$\hat{a}_{\varepsilon, N_k(K)}(t, x) = a_\varepsilon(t, x) |_{N_k(K)} / \bar{a}_{N_k(K)}(t)$$

the locally scaled version of a_ε . Similar to [16, 17], we define for each element $K \in \mathcal{T}_H$ the local error indicator

$$E_K(a_\varepsilon^i, a_\varepsilon^n)^2 = \|\hat{a}_\varepsilon^i(\hat{a}_\varepsilon^n)^{-1}\|_{L^\infty(K)} \sum_{K' \in N_k(K)} \|\hat{a}_\varepsilon^i\|^{-1/2} (\hat{a}_\varepsilon^i - \hat{a}_\varepsilon^n) (\hat{a}_\varepsilon^n)^{-1/2} \|_{L^\infty(K')}^2 \cdot \max_{v|_K, v \in V_H} \frac{\|(\hat{a}_\varepsilon^i)^{1/2} (\chi_K \nabla v - \nabla R_{f,k,K}^i v)\|_{L^2(K')}}{\|(\hat{a}_\varepsilon^i)^{1/2} \nabla v\|_{L^2(K)}^2},$$

where χ_K denotes the characteristic function of K . We emphasize that we consider locally scaled versions of the coefficients in contrast to the original indicators [17]. This scaling is important in the present setting of time-dependent coefficients: As discussed in Remark 2.1, the correctors and multiscale spaces do not need to change over time in the case of coefficients with “tensor-product structure”, i.e., $a_\varepsilon(t, x) = a_{1,\varepsilon}(x) a_2(t)$. The local error indicator defined above reflects this fact in the sense that $E_K(a_\varepsilon^i, a_\varepsilon^n) = 0$ for all K , i and n for such tensor-product coefficients a_ε .

Remark 4.2. We choose to scale the coefficient by dividing with its local average. Other scalings, such as the local minimum or maximum, are equally possible. To extend the procedure to matrix-valued coefficients, one can, for instance, scale with the local average of the trace of a_ε .

We now explain the adaptive algorithm which we illustrate for the LOD stiffness matrix \underline{A}^n in the n th time step. For the first time step, all correctors $\widehat{R}_{f,k} = R_{f,k}^1$ are computed based on $\widehat{a}^1 = a_\varepsilon(t_1, \cdot)$, as described in the previous section. In the subsequent time steps, we evaluate $E_K(\widehat{a}^{n-1}, a_\varepsilon^n)$ for all elements K . Given a prescribed tolerance \mathbf{tol} , we mark all elements with $E_K(\widehat{a}^{n-1}, a_\varepsilon^n) \geq \mathbf{tol}$ and compute a new corrector $R_{f,k,K}^n$ for these elements based upon a_ε^n . Otherwise, the available corrector from the previous time step(s) is used. We then set

$$\widehat{R}_{f,K,k}^n = \begin{cases} R_{f,k,K}^n, & K \text{ marked,} \\ \widehat{R}_{f,k,K}^{n-1}, & \text{else,} \end{cases} \quad \text{and} \quad \widehat{a}_K^n = \begin{cases} a_\varepsilon^n|_{N_k(K)}, & K \text{ marked,} \\ \widehat{a}_K^{n-1}, & \text{else,} \end{cases}$$

and assemble the stiffness matrix contributions as

$$(\widehat{A}_K)_ij^n = \left(\widehat{a}_K^n \nabla \lambda_i \mid \nabla (\text{Id} - \widehat{R}_{f,k,K}^n) \lambda_j \right)_{N_k(K)}.$$

This simply means that the LOD stiffness matrix is defined as a mixture of newly computed correctors as well as local coefficients of the current time step and reused correctors and local coefficients of previous time step(s). A similar procedure can be applied to calculate the other LOD matrices if necessary. Finally, we note that in the extreme cases $\mathbf{tol} = 0$ or $\mathbf{tol} = \infty$, we obtain the Petrov–Galerkin variant of the method from Section 2.2 or a time-stepping with fixed multiscale space based upon $a(t_1, \cdot)$, respectively.

Remark 4.3 (Practical choice of \mathbf{tol}). *Since the absolute value of the error indicator is hard to predict in practice, we suggest the following choice of the tolerance that is also used in our numerical experiments: Fix a tolerance factor $\zeta_{\mathbf{tol}} \in [0, 1]$ and set the tolerance in the n th time step to*

$$\mathbf{tol} = \left(\min_{K \in \mathcal{T}_H} E_K^n \right) + \zeta_{\mathbf{tol}} \left(\max_{K \in \mathcal{T}_H} E_K^n - \min_{K \in \mathcal{T}_H} E_K^n \right),$$

where $E_K^n = E_K(\widehat{a}^{n-1}, a_\varepsilon^n)$ denotes the error indicator in the n th step.

It was shown in [17] that $R_{f,k,K}^n - \widehat{R}_{f,k,K}^n$ can be bounded by $E_K(\widehat{a}^n, a_\varepsilon^n)$ and thereby by \mathbf{tol} . Similar to the estimate for the consistency error in [16, Thm. 4.1], one can show that

$$\|\underline{A}^n - \widehat{A}^n\| \lesssim k^{d/2} \mathbf{tol}$$

holds for all n in a suitable matrix norm.

Let $\widehat{y}_{k,\text{ms}}^n \in (1 - \widehat{R}_{f,k}^n) \mathcal{X}_H$ be the LOD solution computed with the adaptive update strategy. From Theorem 2.2 and a perturbation argument, we expect the following error estimate

$$\|\widehat{y}_{k,\text{ms}}^n - y_h^n\|_{\mathcal{X}} \leq \mathcal{C}_{u,f} e^{\mathcal{C}at_n} (\tau + H + \mathbf{tol}).$$

In fact, our numerical experiments show that the LOD with adaptive update strategy still converges with (spatial) rate H if `tol` is chosen small enough and consequently the consistency error is sufficiently small in comparison to the discretization error.

5 Numerical examples

In this section, we illustrate the theoretical error estimate and the adaptive update strategy by numerical examples. We implemented the Petrov–Galerkin method with the implicit midpoint rule as the time integration scheme using the python module `gridlod` [15]. The code to reproduce the examples below is publicly available at <https://github.com/BarbaraV/gridlod-timedependent>.

Throughout the experiments, we consider the wave equation with time-dependent multiscale coefficients on the spatial domain $\Omega = [0, 1]^2$ and for the time interval $[0, T]$ with final time $T = 1$. We always use homogeneous initial conditions, i.e., $u^0 = 0$ and $v^0 = 0$. The numerical experiments study the relative error between a finescale finite element (reference) solution and the LOD solution measured in the energy norm of \mathcal{X} at final time $T = 1$.

5.1 Spatial and temporal convergence

In our first numerical experiment, we illustrate spatial and temporal convergence rates of the LOD where all correctors are updated in every time step. We choose a periodic time-dependent multiscale coefficient as

$$a_\varepsilon(t, x) = (3 + \sin(2\pi \frac{x_1}{\varepsilon}) + \sin(2\pi t))(3 + \sin(2\pi \frac{x_2}{\varepsilon}) + \sin(2\pi t))$$

with $\varepsilon = 2^{-7}$ and compare two right-hand sides with different spatial regularity, namely

$$f_1(t, x) = \begin{cases} 20t + 230t^2, & x_1 > 0.4, \\ 100t + 2300t^2, & x_1 < 0.4, \end{cases}$$

and

$$f_2(t, x) = 20t(x_1 - x_1^2)(x_2 - x_2^2) + 230t^2(x_1 - x_1^2 + x_2 - x_2^2).$$

Note that $f_1 \in C^\infty(0, T; L^2(\Omega))$ and $f_2 \in C^\infty(0, T; H^1(\Omega))$. The reference solution is computed using the finite element method on a fine mesh with mesh width $h = 2^{-9}$ and the implicit midpoint rule with step size $\tau = 2^{-7}$.

We first fix $\tau = 2^{-7}$ for the LOD and study the spatial convergence on meshes with $H = 2^{-2}, 2^{-3}, \dots, 2^{-6}$ and $k = 1, 2, 2, 3, 3$. Figure 5.1 (left) shows that for f_1 , we obtain a bit more than linear convergence (rate of about $H^{3/2}$) and for f_2 , the convergence is even of quadratic order. Note that f_1 fulfills the regularity and compatibility requirements for our theoretical error estimates and the results underline the spatial convergence rates predicted. Slightly more than linear convergence was also observed in numerical experiments for the autonomous wave equation, cf. [30]. The better rate for f_2 is explained by its higher spatial regularity $H^1(\Omega)$ as also shown theoretically in the time-invariant

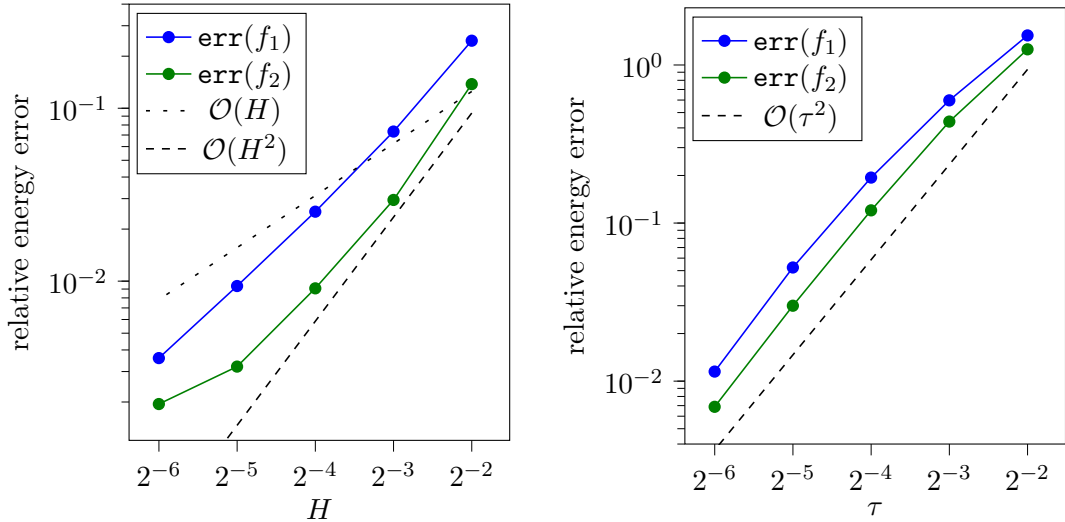


Figure 5.1: Convergence of the relative energy error for the experiments of Section 5.1, left: spatial convergence, right: temporal convergence.

case [2]. These refined error estimates may carry over to the present non-autonomous case. The slower convergence for the smallest H for f_2 can probably be cured by a larger choice of k .

To study the temporal convergence, we fix $H = 2^{-6}$ and $k = 3$ and vary $\tau = 2^{-2}, 2^{-3}, \dots, 2^{-6}$. Figure 5.1 (right) shows that we obtain a quadratic rate in τ for both right-hand sides. This is the expected result for the implicit midpoint rule, cf. Remark 2.5. Altogether, this experiment clearly underlines the theoretically expected convergence rates for the LOD energy error when all correctors are updated in every step.

5.2 Adaptive update strategy

We now study the adaptive update strategy presented in Section 4.2 and its influence on the energy error. In the following we focus on the spatial convergence for fixed tolerance as well as the dependence of the error on the chosen tolerance. We compare different multiscale coefficients, which are discontinuous in space. We choose as right-hand side

$$f(t, x) = \sin(\pi x_1) \sin(\pi x_2) (5t + 50t^2),$$

which has the same regularity properties as f_2 in the first example. The reference finite element solution is again computed with $h = 2^{-9}$ and $\tau = 2^{-7}$.

The first coefficient is

$$a_1(t, x) = (1 + 0.5 \cos(9t)) a_{\text{disc}}(x), \quad \text{with} \quad a_{\text{disc}}(x) = \begin{cases} 10, & \frac{x}{\varepsilon} \in [0.25, 0.75]^2, \\ 1, & \text{else,} \end{cases}$$

with $\varepsilon = 2^{-7}$. The coefficient a_{disc} is visualized in Figure 5.2 (left), where we chose $\varepsilon = 2^{-5}$ for better visibility. The structure of a_1 allows us to keep the correctors constant

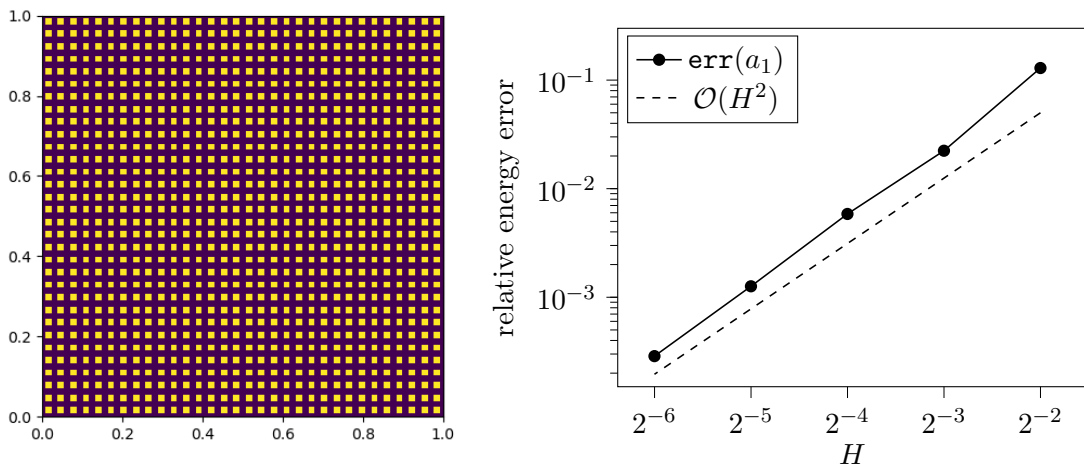


Figure 5.2: First experiment in Section 5.2: coefficient a_{disc} for $\varepsilon = 2^{-5}$ (left – blue is 1 and yellow is 10) and spatial convergence of the LOD method for a_1 (right).

in time, cf. Remark 2.1, and only multiply the stiffness matrix with the global value $(1 + 0.5 \cos(9t_{n+1/2}))$ in the n th time step. Hence, in this case the method is as efficient as for time-independent coefficients: We can pre-compute the multiscale basis (or the LOD stiffness matrix) and only have to solve a small linear system in each time step. Figure 5.2 (right) shows the spatial convergence for $H = 2^{-2}, 2^{-3}, \dots, 2^{-6}$, $k = 1, 2, 2, 3, 3$, and $\tau = 2^{-7}$, where we observe a quadratic rate as expected due to the spatial regularity of the right-hand side, as discussed in the previous section. We emphasize that it is crucial to use the error indicator with scaled coefficients in this example since otherwise unnecessary updates of the correctors would be triggered.

Now we consider two coefficients without this “tensor-product” structure in space and time to study the influence of the update strategy. We consider

$$a_2(t, x) = \begin{cases} (1 + 0.5 \cos(9t))a_{\text{disc}}(x), & x \in [0.25, 0.75]^2, \\ a_{\text{disc}}(x), & \text{else,} \end{cases}$$

and

$$a_3(t, x) = a_{\text{disc}}(x) + 1 + 0.5 \cos(9t)$$

with the same a_{disc} as for a_1 . We first update all correctors where the indicator has a value larger than the mean value of all error indicators, i.e., $\zeta_{\text{tol}} = 0.5$ as explained in Remark 4.3. The spatial convergences for $H = 2^{-2}, 2^{-3}, 2^{-4}, 2^{-5}$, $k = 1, 2, 2, 3$, and $\tau = 2^{-6}$ are shown in Figure 5.3 (left). Except for the last mesh size, we still obtain at least linear convergence in H , while especially for a_2 we even have quadratic convergence. The theoretically expected order is $\mathcal{O}(H^2)$ if we update all correctors in every time step and slower linear convergence as well as the stagnation for the last mesh size can be explained by the dominance of the updating error. Still, the relative energy error is only a few percent for mesh sizes of $H = 2^{-4}$ or $H = 2^{-5}$, which is satisfactory in many

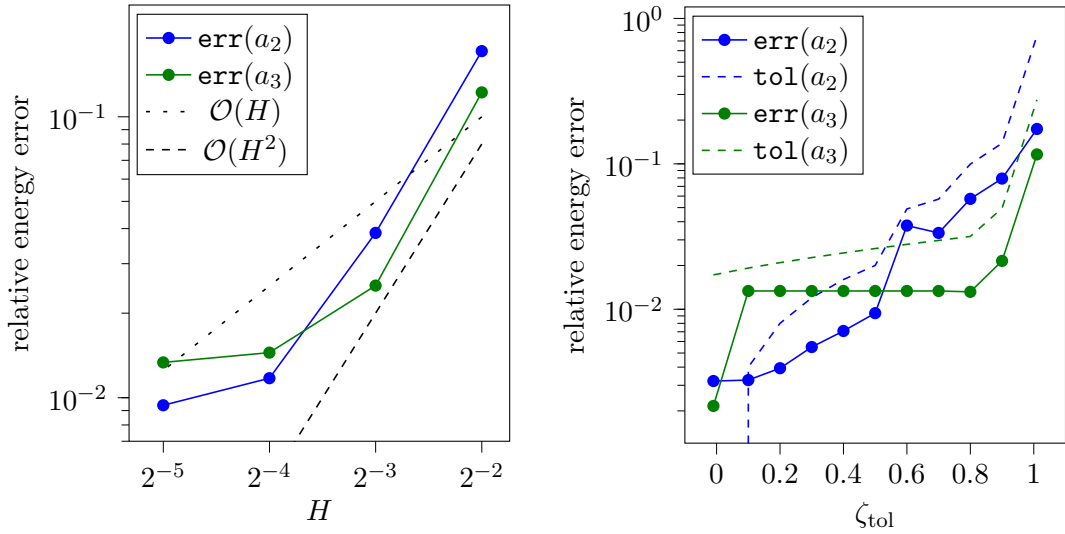


Figure 5.3: Second experiment in Section 5.2: spatial convergence for fixed tolerance factor 0.5 (left) and error as well as maximal tolerance in dependence on tolerance factor (right).

applications. Moreover, we emphasize that by the adaptive strategy we only need to update 14.1% or 50.6% of the correctors on average in every step for a_2 or a_3 , respectively. As the main computation time is spent on the assembly of the LOD stiffness matrices, such an adaptive update strategy reduces the computational complexity considerably in comparison to the “perfect” case where correctors are computed in every time step. The smaller update percentage for a_2 is caused by the time modulation acting only in some part of the domain. Figure 5.3 (right) shows how the maximal tolerance (over all time steps) as well as the energy error evolve for different choices of the tolerance factor for fixed $H = 2^{-5}$ and $k = 3$. We see that tolerance factors around 0.5 seem to provide a good compromise between computational efficiency and accuracy.

On the whole, we conclude that in all cases considered, we could achieve relative energy errors of only a few percent already using moderate mesh widths and time step sizes and updating only about half of the correctors on average in every time step.

Conclusion

In this work, we analyzed a multiscale method in the spirit of the localized orthogonal decomposition for wave equations with time-dependent multiscale coefficients. The method constructs (coarse) multiscale spaces in each time step. We rigorously proved convergence rates in the mesh width and the time step size for spatially rough coefficients. For this, we showed the exponential decay of the time derivative of the multiscale basis functions. To obtain a computationally efficient method, we proposed an adaptive update strategy for the multiscale basis based upon an appropriate error indicator. The

presented numerical examples have underlined the theoretical findings and in particular show that small updates in every time step and moderate choices of the oversampling parameter are already sufficient to obtain reasonable approximations.

We expect the methodology and the techniques of error analysis to carry over to other problem classes as well, for instance parabolic problems with space- and time-dependent coefficients. Further, by considering several previous time steps in the adaptive update strategy, even more coefficient classes such as (almost) time-periodic coefficients may become treatable in the future.

References

- [1] A. Abdulle and M. J. Grote. Finite element heterogeneous multiscale method for the wave equation. *Multiscale Model. Simul.*, 9(2):766–792, 2011.
- [2] A. Abdulle and P. Henning. Localized orthogonal decomposition method for the wave equation with a continuum of scales. *Math. Comp.*, 86(304):549–587, 2017.
- [3] H. Ammari and E. O. Hiltunen. Time-dependent high-contrast subwavelength resonators. arXiv preprint 2012.10274, 2020.
- [4] G. Bal, M. Fink, and O. Pinaud. Time-reversal by time-dependent perturbations. *SIAM J. Appl. Math.*, 79(3):754–780, 2019.
- [5] L. A. Bales. Higher order single step fully discrete approximations for second order hyperbolic equations with time dependent coefficients. *SIAM J. Numer. Anal.*, 23(1):27–43, 1986.
- [6] L. A. Bales, V. A. Dougalis, and S. M. Serbin. Cosine methods for second-order hyperbolic equations with time-dependent coefficients. *Math. Comp.*, 45(171):65–89, 1985.
- [7] S. C. Brenner and L. R. Scott. *The mathematical theory of finite element methods*, volume 15 of *Texts in Applied Mathematics*. Springer, New York, third edition, 2008.
- [8] D. Elfverson, V. Ginting, and P. Henning. On multiscale methods in Petrov-Galerkin formulation. *Numer. Math.*, 131(4):643–682, 2015.
- [9] B. Engquist, H. Holst, and O. Runborg. Multi-scale methods for wave propagation in heterogeneous media. *Commun. Math. Sci.*, 9(1):33–56, 2011.
- [10] D. Gallistl, P. Henning, and B. Verfürth. Numerical homogenization of H(curl)-problems. *SIAM J. Numer. Anal.*, 56(3):1570–1596, 2018.
- [11] D. Gallistl and D. Peterseim. Stable multiscale Petrov–Galerkin finite element method for high frequency acoustic scattering. *Comput. Methods Appl. Mech. Engrg.*, 295:1–17, 2015.

- [12] S. Geever and R. Maier. Fast mass lumped multiscale wave propagation modelling. arXiv preprint 2104.08346, 2021.
- [13] G. Gilardi. Teoremi di regolarità per la soluzione di un'equazione differenziale astratta lineare del secondo ordine. *Ist. Lombardo Accad. Sci. Lett. Rend. A*, 106:641–675, 1972.
- [14] X. Guo, Y. Ding, Y. Duan, and X. Ni. Nonreciprocal metasurface with space-time phase modulation. *Light: Science & Applications*, 8(1):123, 2019.
- [15] F. Hellman and T. Keil. Gridlod. <https://github.com/fredrikhellman/gridlod>, 2019. GitHub repository, commit 0ed4c096df75040145978d48c5307ef5678efed3.
- [16] F. Hellman, T. Keil, and A. Målqvist. Numerical upscaling of perturbed diffusion problems. *SIAM J. Sci. Comput.*, 42(4):A2014–A2036, 2020.
- [17] F. Hellman and A. Målqvist. Numerical homogenization of elliptic PDEs with similar coefficients. *Multiscale Model. Simul.*, 17(2):650–674, 2019.
- [18] P. Henning and A. Målqvist. Localized orthogonal decomposition techniques for boundary value problems. *SIAM J. Sci. Comput.*, 36(4):A1609–A1634, 2014.
- [19] P. Henning and A. Persson. Computational homogenization of time-harmonic Maxwell's equations. *SIAM J. Sci. Comput.*, 42(3):B581–B607, 2020.
- [20] P. Henning and D. Peterseim. Oversampling for the multiscale finite element method. *Multiscale Model. Simul.*, 11(4):1149–1175, 2013.
- [21] M. Hochbruck and B. Maier. Error analysis for space discretizations of quasilinear wave-type equations. CRC 1173 Preprint 2021/2, Karlsruhe Institute of Technology, 2021.
- [22] L. Jiang and Y. Efendiev. A priori estimates for two multiscale finite element methods using multiple global fields to wave equations. *Numer. Methods Partial Differential Equations*, 28(6):1869–1892, 2012.
- [23] L. Jiang, Y. Efendiev, and V. Ginting. Analysis of global multiscale finite element methods for wave equations with continuum spatial scales. *Appl. Numer. Math.*, 60(8):862–876, 2010.
- [24] J. Li, C. Shen, X. Zhu, Y. Xie, and S. A. Cummer. Nonreciprocal sound propagation in space-time modulated media. *Physical Review B*, 99(14):144311, 2019.
- [25] P. Ljung, A. Målqvist, and A. Persson. A generalized finite element method for the strongly damped wave equation with rapidly varying data. *ESAIM Math. Model. Numer. Anal.*, 55(4):1375–1403, 2021.
- [26] A. Målqvist and A. Persson. Multiscale techniques for parabolic equations. *Numer. Math.*, 138(1):191–217, 2018.

- [27] A. Målqvist and D. Peterseim. Localization of elliptic multiscale problems. *Math. Comp.*, 83(290):2583–2603, 2014.
- [28] A. Målqvist and D. Peterseim. *Numerical Homogenization by Localized Orthogonal Decomposition*, volume 5 of *SIAM Spotlights*. Society for Industrial and Applied Mathematics (SIAM), Philadelphia, PA, 2021.
- [29] B. Maier. Error analysis for full discretizations of quasilinear wave-type equations with two variants of the implicit midpoint rule. CRC 1173 Preprint 2021/24, Karlsruhe Institute of Technology, 2021.
- [30] R. Maier and D. Peterseim. Explicit computational wave propagation in micro-heterogeneous media. *BIT*, 59(2):443–462, 2019.
- [31] R. Maier and B. Verfürth. Multiscale scattering in nonlinear Kerr-type media. arXiv preprint 2011.09168, 2020.
- [32] V. Nikolić and B. Wohlmuth. A priori error estimates for the finite element approximation of Westervelt’s quasi-linear acoustic wave equation. *SIAM J. Numer. Anal.*, 57(4):1897–1918, 2019.
- [33] H. Owhadi and L. Zhang. Numerical homogenization of the acoustic wave equations with a continuum of scales. *Comput. Methods Appl. Mech. Engrg.*, 198(3-4):397–406, 2008.
- [34] D. Peterseim. Eliminating the pollution effect in Helmholtz problems by local sub-scale correction. *Math. Comp.*, 86(305):1005–1036, 2017.
- [35] D. Peterseim and M. Schedensack. Relaxing the CFL condition for the wave equation on adaptive meshes. *J. Sci. Comput.*, 72(3):1196–1213, 2017.
- [36] D. Peterseim and B. Verfürth. Computational high frequency scattering from high-contrast heterogeneous media. *Math. Comp.*, 89(326):2649–2674, 2020.